Analytica Chimica Acta 1207 (2022) 339811

Contents lists available at ScienceDirect

Analytica Chimica Acta

journal homepage: www.elsevier.com/locate/aca

A highly sensitive fluorometric biosensor for Fumonisin B1 detection based on upconversion nanoparticles-graphene oxide and catalytic hairpin assembly

Yingkai Qin [a, 1], Shuang Li [a, b, 1], Yu Wang [a], Yuan Peng [a], Dianpeng Han [a], Huanying Zhou [a], Jialei Bai [a], Shuyue Ren [a], Sen Li [a], Ruipeng Chen [a], Tie Han [a, **], Zhixian Gao [a, *]

[a] Tianjin Institute of Environmental and Operational Medicine, Tianjin Key Laboratory of Risk Assessment and Control Technology for Environment and Food Safety, No. 1 Da Li Road, Tianjin, 300050, PR China
[b] Academy of Medical Engineering and Translational Medicine, Tianjin University, No. 92 Weijin Road, Tianjin, 300072, PR China

HIGHLIGHTS

- CHA enhanced the detection sensitivity of UCNPs and reduced the effect of surface self-quenching of UCNPs.
- CHA regulated the FRET efficiency between UCNPs and GO, inducing the recovery of the GO quenched fluorescence signal.
- The proposed biosensor exhibited high satisfactory specificity for the detection of FB1 in imported food.
- High throughput fluorescence detection can be achieved by using different UCNPs, aptamers and CHA cycles.

GRAPHICAL ABSTRACT

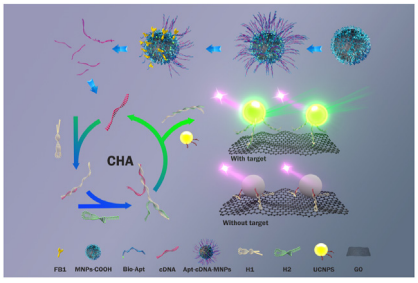

ARTICLE INFO

Article history:
Received 28 January 2022
Received in revised form
24 March 2022
Accepted 4 April 2022
Available online 6 April 2022

Keywords:
Upconversion nanoparticles-graphene oxide
Mycotoxins
Catalytic hairpin assembly
Fluorescence resonance energy transfer
Food safety

ABSTRACT

Fumonisin (FB) is a common mycotoxin in corn, wheat, oats, and their related products. FB1 is the most predominant among fumonisins and is responsible for severe food contamination that may have deleterious effects on public health. Therefore, the demand for achieving sensitive detection of FB1 is becoming more and more pressing. In the present study, a creative biosensor for FB1 detection was developed based on fluorescence resonance energy transfer between upconversion nanoparticles (UCNPs) and graphene oxide (GO) with catalytic hairpin assembly (CHA) target recycling and amplification. In the presence of FB1, UCNPs were bound to the CHA amplification products away from the GO surface. Simultaneously, a strong fluorescence signal was produced at 980 nm (near-infrared light). The correlation between the concentration of FB1 and the fluorescence intensity exhibited a high relevance ($R^2 = 0.9971$) ranging from 0.032 to 500 ng mL^{-1}, and the method reached a considerably low limit of detection (0.0121 ng mL^{-1}). It could be applied for the detection of FB1 in corn, oats, and infant supplements. The sensitive detection of FB1 proves the application potential of this method on food safety

* Corresponding author. Tianjin Institute of Environmental and Operational Medicine, Tianjin Key Laboratory of Risk Assessment and Control Technology for Environment and Food Safety, 1 Da Li Road, Tianjin, 300050, PR China.
** Corresponding author.
E-mail addresses: hantietj@163.com (T. Han), gaozhx@163.com (Z. Gao).
[1] These authors contribute equality to this work.

https://doi.org/10.1016/j.aca.2022.339811

detection. This biosensor can enable high-throughput fungal toxin detection by allowing the use of various aptamers.

1. Introduction

Fumonisin B1 in food is produced mainly by *F. moniliforme* and *F. proliferatum*. This compound plays a pivotal role in global mycotoxin contamination incidents [1]. It can cause the development of animal diseases, such as equine leukomalacia, porcine pulmonary edema syndrome, and rat liver cancer. It also exerts a huge impact regarding the incidence of adverse effects on the breeding industry [2–4]. The International Agency for Research on Cancer (IARC) lists FB1 as a possible human carcinogen (Group 2B) [5,6]. Certain studies have found an inextricable link between the prevalence of esophageal cancer in humans and the concentration of FB1 in the region's crops [7]. In Tanzania, children under 6 months of age are seriously underweight due to breastfeeding with contaminated milk containing FB1 [8]. Iran, France, Bulgaria, Switzerland, and other countries stipulate that the maximum FB1 contamination limit of corn-based breakfast cereals and snacks should be 800 μg kg^{-1}, whereas that of the baby food should be estimated to be 200 μg kg^{-1} [9].

The probability of FB1 pollution is relatively high due to human production and living. In addition, FB1 can bind to other mycotoxins, which further expands the harm to the human body [10]. Therefore, this compound is a perennial concern for the food industry, academic communities, and regulatory authorities. The majority of the methods developed for the quantitative analysis of FB1 include liquid chromatography-mass spectrometry [11], high-performance liquid chromatography [12–14], and enzyme-linked immunosorbent assay [15]. These methods achieve high sensitivity but also exhibit several drawbacks, such as the need for expensive instruments, complex pre-processing, and cumbersome operations, which are primarily unsolved challenges.

In recent years, biosensors based on fluorescence detection have increasingly attracted widespread attention due to their high sensitivity, easy operation, and rapid response [16–19]. For example, the red CdTe quantum dots were modified on the FB1 aptamer and subsequently fixed on the graphene oxide (GO)/ferric oxide nanocomposite [20]. CdTe fluorescence was quenched owing to the fluorescence resonance energy transfer (FRET) between GO and CdTe. FRET is based on the non-radiative energy transfer between the donor and the acceptor based on the electrostatic dipole-dipole interaction [21,22]. FRET occurs when two conditions are met: 1) The emission spectrum of the energy donor and the absorption spectrum peak of the energy acceptor overlap; 2) the distance between the two is less than 10 nm [23–27]. However, quantum dots have a high background value and specific biological toxicity. Therefore, a non-toxic fluorescent material without background signal interference is required to address this problem. UCNPs follow the anti-stokes law of luminescence and can convert low-energy photons into high-energy photons [28–30]. Compared with traditional fluorescent materials, UCNPs are better due to sharp emission peaks, high fluorescence purity, long fluorescence lifetime, absence of interference from background fluorescence, optimal chemical stability, and accessible surface modification [31–36]. Biosensors based on UCNPs have shown excellent detection performance in the detection of biomarkers, such as CEA and AFP [37–39]. However, the fluorescence self-quenching effect caused by surface defects can reduce the fluorescence intensity of upconversion nanomaterials, which is detrimental to their detection sensitivity [40]. Furtherly, through the signal amplification strategy, the detection sensitivity has been greatly improved accordingly.

Nucleic acid amplification technologies, one of the signal amplification strategies, have been introduced into the detection field with the virtue of significant signal amplification [41–43], such as hybrid chain reaction (HCR) [44], rolling circle amplification (RCA) [45], strand displacement amplification (SDA) [46], and catalytic hairpin assembly (CHA) [47]. CHA is an efficient, enzyme-free, and minimum-processing-required amplification strategy, which exhibits high potential in improving detection sensitivity [48]. Yin et al. reported the introduction of CHA for the first time in 2008 [49]. Moreover, Li et al. applied CHA in practice in 2011 and achieved a signal amplification effect of 100 times [50]. The CHA reaction generally includes two stable hairpin DNA structures. When the priming strand is present, the loop structure of one hairpin (H1) is unfolded, exposing the sticky end that is complementary to the other hairpin (H2) and resulting in a double-stranded DNA molecule (dsDNA) of H1+H2. Since the initiator strand continuously opens the ring structure of H1 in the system, it promotes the generation of dsDNA, thus achieving signal amplification [51].

In the present study, a new signal amplification strategy was proposed for the detection of FB1, making up for the sensitivity lost by UCNPs due to self-quenching simultaneously. The detection of FB1 in food was accomplished by leveraging CHA and UCNPs-GO. The FB1 aptamer and complementary DNA strands were immobilized on the magnetic microspheres (MMPs) through the interaction of streptavidin-biotin. Following the specific binding of FB1 to the aptamer, the complementary DNA strands, collected by magnetic separation, were utilized as the priming strand to undergo CHA amplification. Subsequently, the UCNPs were conjugated with the amplified dsDNA and separated from the GO surface. Finally, quenching of the UCNPs fluorescence was restored. The detection method appeared to demonstrate broad application prospects in the detection of FB1 due to its high sensitivity, wide detection range, strong specificity, and low cost.

2. Experimental section

2.1. Reagents and apparatus

All aqueous solutions were prepared using ultrapure water (Milli-Q, 18MΩ, Millipore). $YCl_3 \cdot 6H_2O$, $YbCl_3 \cdot 6H_2O$, $ErCl_3 \cdot 6H_2O$, $FeCl_3 \cdot 6H_2O$, CH_3COONa, $Na_3C_6H_5O_7$, oleic acid (OA), 1-octadecene(ODE), and polyethyleneimine (PEI) were purchased from Shanghai Yien Chemical Technology Co., Ltd. Ammonium fluoride, ethylene glycol, sodium hydroxide, methanol, and cyclohexane were purchased from Macleans Biochemical Technology Co., Ltd. (all of analytical grade). Glutaraldehyde (50%) and GO were purchased from Aladdin Biochemical Technology Co., Ltd. Streptavidin was obtained from Shanghai Yuanye Biotechnology Co., Ltd. PBS buffer was purchased from Beijing Solarbio Technology Co., Ltd. FB1 standard, zearalenone (ZEN) standard, T-2 toxin (T-2) standard, ochratoxin A (OTA) standard, aflatoxin B1 (AFB1) standard, aflatoxin M1 (AFM1) standard products, and aflatoxin M2 (AFM2) standard products were acquired from Shandong Lvdu

Biotechnology Co., Ltd. All DNA oligonucleotides were synthesized and purified utilizing high-performance liquid chromatography by Shanghai Sangon Biological Co., Ltd. The synthetic DNA sequences are shown in Table S1.

The morphologies of the materials were analyzed by JEM 2100 Transmission electron microscope (TEM, Japan Electron Optics Laboratory, Japan) and SU 3500 Scanning electron microscope (SEM, Hitachi High-Technologies Corporation). The Fourier transform infrared (FTIR) spectroscopy was measured with the NicoletiS50 spectrophotometer (Thermo Fisher Scientific, USA). The fluorescence intensity was recorded using F97 pro fluorescence spectrophotometer (Shanghai Lengguang Technology Co.,Ltd, Shanghai, China) with a 980 nm semiconductor laser (Hi-Tech Optoelectronics Co., Ltd, Beijing, China). The UV absorption spectrum was recorded by TU-1901 UV−vis spectrophotometer (Beijing Purkinje General Instrument Co.,Ltd,Beijing, China). The Zeta potential was measured by Mastersizer 3000 (Malvern PANalytical Co., Ltd, England) and the Atomic force microscopy (AFM) Spectrum was recorded by MultiMode 8 (BrukerDaltonics Inc., USA).

2.2. Synthesis and surface modification of magnetic microspheres

The MMPs were synthesized according to the previously published methods [52]. $FeCl_3 \cdot 6H_2O$ (1.3 g) and CH_3COONa (3.5 g) were mixed in 40 mL ethylene glycol prior to the addition of $Na_3C_6H_5O_7$ (2.4 g). The solution was mechanically stirred for 0.5 h and subsequently transferred to a 50 mL PTFE-lined stainless steel autoclave. The autoclave was kept at 210 °C for 15 h and subsequently cooled down to room temperature. The product was purified by repeated washing with ethanol and then dried at 60 °C for 8 h.

Following activation of carboxylated magnetic microspheres (500 μL, 10 mg mL^{-1}) by EDC (50 μL, 50 mg mL^{-1}, pH 5.0) and NHS (50 μL, 50 mg mL^{-1}, pH 5.0) for 0.5 h, streptavidin (200 μL, 1 mg mL^{-1}) was used to react with these compounds at room temperature by continuous shaking for 2 h. Eventually, the product was washed three times with PBS buffer and centrifuged.

2.3. Synthesis and surface modification of UCNPs

A solvothermal method was applied to synthesize the UCNPs [53]. 1 mmol $RECl_3 \cdot 6H_2O$ (Y:Yb: Er = 80:18:2) was dissolved in 9 mL OA and 15 mL ODE. Subsequently, the solution was placed into a 100 mL three-necked flask and heated to 120 °C for vacuum degassing and water removal. The solution was allowed to cool down to room temperature and 10 mL methanol with 4 mmol NH_4F and 2.5 mmol NaOH was added dropwise. The final solution was stirred at 25 °C for 0.5 h and heated to 120 °C for condensation and reflux to remove the methanol. Finally, it was heated to 320 °C for 1.5 h in the presence of nitrogen. Ethanol was added for precipitation following cooling down of the solution to room temperature. The resulting precipitate was purified by centrifugation by washing with cyclohexane at 13,000 rpm. Following three times of washing, drying at 60 °C was performed overnight by vacuum.

The surface modification of UCNPs was carried out by the ligand exchange method [54]. A total of 300 mg polyethyleneimine was dissolved in 5 mL ultrapure water, and 10 mL 2 mg mL^{-1} UCNPs solution (the solvent was cyclohexane) was added, followed by mechanical stirring for a total 24 h. The precipitate was washed with ethanol and centrifuged at 12,000 rpm. Finally, PEI-UCNPs were obtained by freeze-drying.

2.4. Feasibility verification

The results of CHA amplification were verified by experiments of polyacrylamide gel electrophoresis (PAGE) and by modification of the fluorescent groups on hairpins. cDNA, H1, and H2 were heated at 95 °C for 5 min, and the heating temperature was slowly lowered to room temperature. The solution was diluted with PBS to 5 μM. The hybridization reactions were performed at 37 °C for 40 min. PAGE was carried out using 1 × TBE buffer. The voltage used was 120 V and the run time used was 60 min. The electropherograms were acquired on the IQ350 imaging system following staining of the gel with Genegreen for 20 min.

The fluorescent H2 (F−H2) was annealed in a PBS buffer solution over a temperature gradient from 95 °C to 37 °C. It was diluted to 1 μM with PBS and incubated with cDNA, H1 (both 1 μM) in the dark for 1 h. The fluorescence intensity was measured at 520 nm.

2.5. UCNPs-GO biosensor detection method

The streptavidin-modified MMPs (1 μL, 10 mg mL^{-1}) and biotinylated FB1 aptamer (210 pmol) were incubated overnight at 37 °C to obtain the Apt-MMP solution. Subsequently, 200 μL Apt-MMP solution was hybridized with excess cDNA at 37 °C for 1 h cDNA-Apt-MMPs were obtained and resuspended in PBS buffer (200 μL) following magnetic separation. FB1 standards (100 μL) with different concentrations were added in the cDNA-Apt-MMP solution at 37 °C for 0.5 h. The supernatant (180 μL) was obtained by magnetic separation, which was subsequently mixed with H1 (10 μL, 100 μM) and H2 (10 μL, 100 μM) for hybridization at 37 °C for 1 h.

PEI-UCNPs (200 μL, 2 mg mL^{-1}) and 25% glutaraldehyde solution (100 μL) were shaken and allowed to react at room temperature for 2 h. Following washing (two times) with PBS buffer and centrifugation, the product was resuspended in PBS buffer (180 μL). The aminated ssDNA (20 μL, 10 μM) was slowly shaken with the product overnight at 1 °C. The mixture was washed, centrifuged, and resuspended in PBS buffer (200 μL) to obtain the ssDNA-UCNPs.

The ssDNA-UCNPs (100 μL, 2 mg mL^{-1}) were combined with the hybridization mixture of H1 and H2 at 37 °C for 1 h and the GO solution (100 μL, 0.6 mg mL^{-1}) was added. The fluorescence of the mixture was monitored at an excitation and emission wavelength of 980 and 546 nm, respectively.

The samples used were all imported corn flour, oat flour, and infant supplements purchased from the Taobao website. A total of 1 g of these samples was mixed with 10 mL extraction solvent {acetonitrile: water, 1:1 (v:v) } containing diverse concentrations (final concentration of 0.1, 1, 10 ng mL^{-1}) of FB1. The samples were centrifuged at 13,000 rpm and the supernatant was obtained. A total of 10 μL supernatant was mixed with 990 μL PBS buffer evenly for subsequent detection.

3. Results and discussion

3.1. Detection principle

The principle of the UCNPs-GO sensor was based on the CHA amplification. As shown in Fig. 1, the FB1 aptamer and its cDNA were immobilized on the surface of MMPs through the action of streptavidin-biotin. In the absence of FB1, the cDNA would not trigger the CHA reaction. The surface of the UCNPs was connected to the ssDNA, which interacted with the unsaturated structure of GO and was close to its surface, resulting in FRET and fluorescence quenching. When FB1 bound specifically to the aptamer, enrichment of the detached cDNA was achieved by magnetic separation. As a result of hybridization between the complementary region of the cDNA and the exposed toehold H1, H1 unfolded to form the intermediate product of the H1+cDNA complex. Furthermore, the exposed portion of H1 triggered another assembly reaction with H2, which then unfolded to form the H1+cDNA + H2 complex.

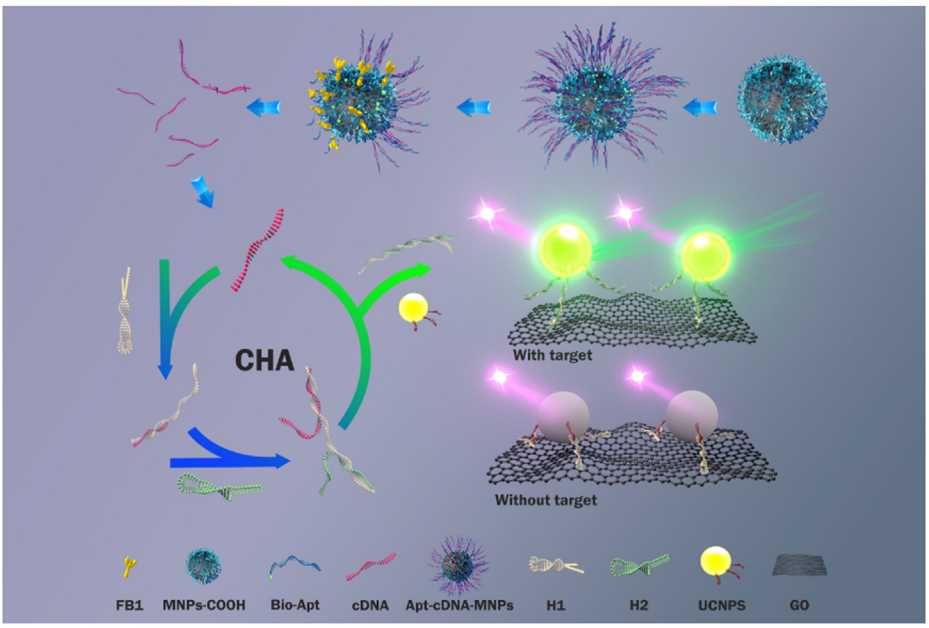

Fig. 1. Schematic diagram of the principle of a highly sensitive fluorometric biosensor for FB1 detection based on upconversion nanoparticles-graphene oxide and catalyzed hairpin assembly.

Eventually, the branch migration was triggered by H2, leading to the release of cDNA and the formation of stable H1+H2 dsDNA. The released cDNA can trigger the next CHA cycle, which led to the formation of large amounts of H1+H2 dsDNAs. These dsDNAs were captured by the ssDNA-UCNPs due to the principle of complementary base pairing. An emergent result was present indicating that the UCNPs were detached from the surface of the GO, leading to the increase in fluorescence.

3.2. Characterization

The SEM images of the resultant carboxylated MMPs demonstrated that the average diameter was approximately 2 μm in Fig. S1. They possessed an excellent magnetic separation ability (magnetic separation in half a minute). The surface of carboxylated MMPs was modified with streptavidin, as noted in Fig. 2 (A). The UV−visible absorption spectrum of streptavidin and the UV−visible absorbance of the supernatant following modification with streptavidin were measured. The typical UV absorption peak of streptavidin at 280 nm demonstrated a visible drop, indicating only a small amount of streptavidin in the supernatant. Furthermore, it was confirmed that the carboxyl groups on MMPs activated by EDC and NHS were covalently coupled with streptavidin. Accordingly, the Biotin-modified FB1 aptamers were bound to the surface of MMPs due to the specific recognition of streptavidin-biotin. The Zeta potential in Fig. 2 (B) was decreased from −27 mV (the carboxylated MMPs) to −33 mV (Apt-MMPs) owing to the assembly of the negatively charged FB1 aptamer. The negative potential of the carboxylated MMPs was increased due to the carboxylate ion. Therefore, the Apt-MMPs used to seize the target FB1 in the samples were successfully prepared with optimal storage performance.

The FT-IR spectra were also performed in Fig. 2 (C). As expected, the bands at 2919 and 2846 cm^{-1} were respectively assigned to the asymmetric and symmetric methylene group (−CH_2−) stretching vibrations in OA, while the peaks corresponding to the asymmetric and symmetric stretching vibration of the carboxylic group (-COOH) were observed at 1606 and 1457 cm^{-1}, respectively (Black curve). Following the coating of a layer of PEI on the surface of the UCNPs, the characteristic vibration bands of −NH−, which represented tensile and bending vibrations, were visible at 3452 and 1605 cm^{-1}. Moreover, the tensile vibration of −CN− in PEI was observed at 1101 cm^{-1} (Red curve). All of these procedures indicated that OA-UCNPs had been functionalized with amino groups to be used in subsequent research. To allow PEI-UCNPs to tag products that were derived from CHA, the ssDNA complementary to CHA products was assembled with PEI-UCNPs. Fig. 2 (B) reflected

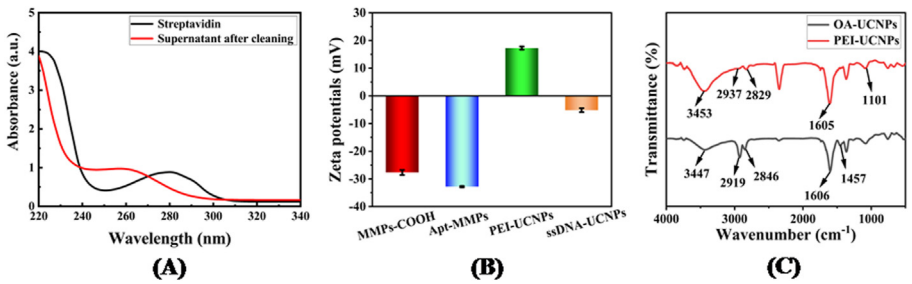

Fig. 2. (A) UV−Vis graphs of the supernatant prior to (black curve) and following (red curve) the coupling of carboxylated MMPs with streptavidin; (B) Zeta potential prior to and following streptavidinylated MMPs coupled with biotinylated FB1 aptamer and prior to and following coupling of PEI-UCNPs to ssDNA; (C) FT-IR of OA-UCNPs (black curve) and PEI-UCNPs (red curve). (For interpretation of the references to colour in this figure legend, the reader is referred to the Web version of this article.)

the change in the Zeta potential prior to and following the coupling of PEI-UCNPs to ssDNA. Since ssDNA exhibited a negative potential and the amino group exhibited a positive potential, a downward trend was noted following coupling, which was also indicative of the successful modification of the amino group.

The oleic acid phase UCNPs (OA-UCNPs) were synthesized via a solvothermal route with a few adjustments. The resultant OA-UCNPs displayed well-defined dispersion and uniform particle size with an interplanar spacing of 0.439 nm, as determined by TEM and HRTEM (High-Resolution transmission electron microscopy) in Fig. 3 (A). Under the irradiation of a 980 nm laser pointer, the OA-UCNPs emitted intense green fluorescence, which was readily available and could be noted directly by the naked eye. The particle size of OA-UCNPs was approximately 30 nm (Fig. 3B). The crystallographic character demonstrated the firm luminescence property of UCNPs as an optical module for signal output. By using the ligand exchange method, the oleic acid groups on the surface of UCNPs were replaced by PEI. Accordingly, a layer of PEI was available to be observed following assembly on the surface of the UCNPs, as shown in Fig. 3(C) and (D).

The TEM images of GO indicated that GO featured curled edges and wrinkles, which were observed in Fig. S3. Simultaneously, it was noted in Fig. S4 that the thickness of GO was approximately 1 nm. Moreover, the thickness of the stacked GO was increased. These results were indicative of the preparation for the following experiments.

3.3. Feasibility study

The detection principle was substantiated to verify the biosensor's feasibility. The aptamer's conformational changes were characterized by circular dichroism (CD). The CD spectra are shown in Fig. S2, and no apparent crests and troughs were observed for the FB1 toxin. In turn, the CD spectra for the aptamer clearly indicated two trough bands at $\lambda = 205$ and 250 nm and a positive peak band at the 280 nm region, which was consistent with previous literature studies. Following the addition of the FB1 toxin, the aforementioned regions were slightly weakened in intensity. However, they maintained a high degree of similarity in the peak locations. It was deduced that the helical structure had changed upon target binding. The selective recognition from the aptamer to the highly concerning FB1 toxin was possible. The UV−visible absorption spectrum of GO was observed in Fig. 4 (A), which exhibited a broad-range high absorption at 400−600 nm. An overlap was noted with the emission spectrum of the UCNPs, indicating the possibility of quenching upconversion fluorescence due to FRET. Fig. 4 (B) demonstrated the extent to which UCNPs bound to different DNAs were quenched by GO, which satisfied an additional condition for FRET.

The results of PAGE indicated the feasibility of the signal amplification strategy in Fig. 4 (C). Lane 1, lane 2, and lane 3 represented H0 (cDNA), H1, and H2, respectively. When H1 was mixed with H0 (lane 4), a new band (H0−H1) appeared, indicating that the

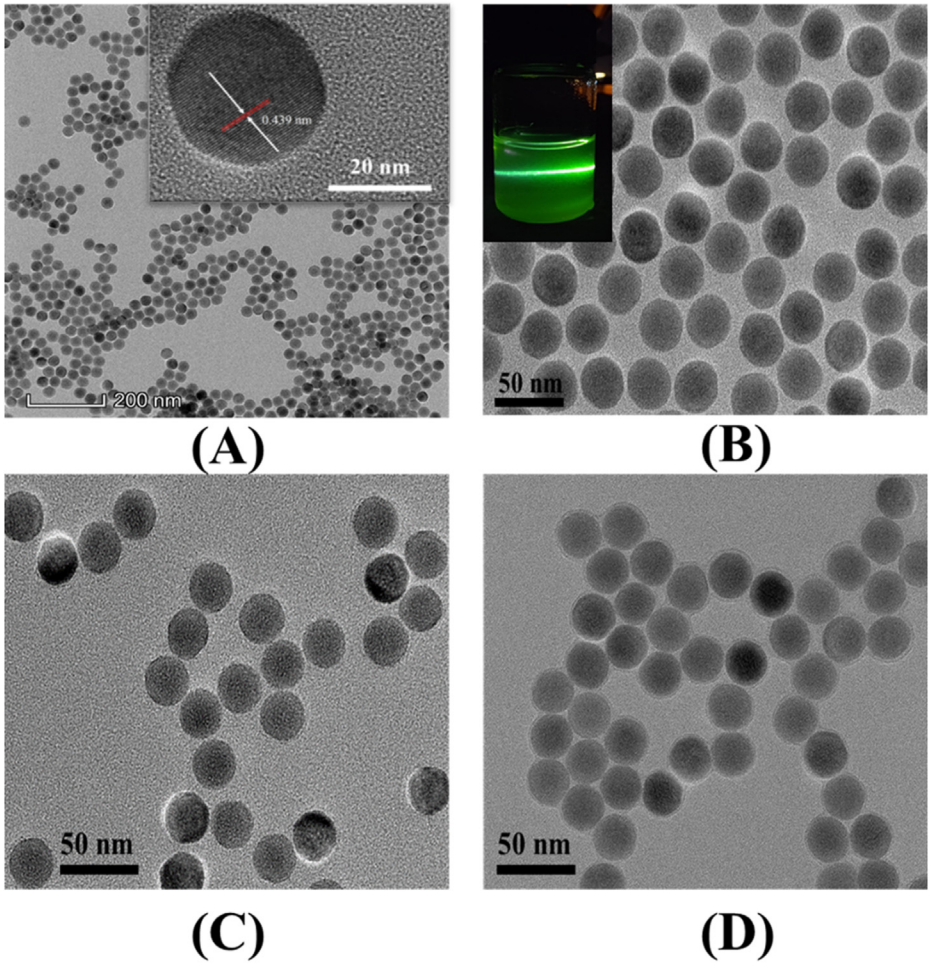

Fig. 3. (A) TEM images of OA-UCNPs and HRTEM image of OA-UCNPs; (B) OA-UCNPs dispersed in cyclohexane; (C) and (D) are the TEM images prior to and following PEI modification, respectively.

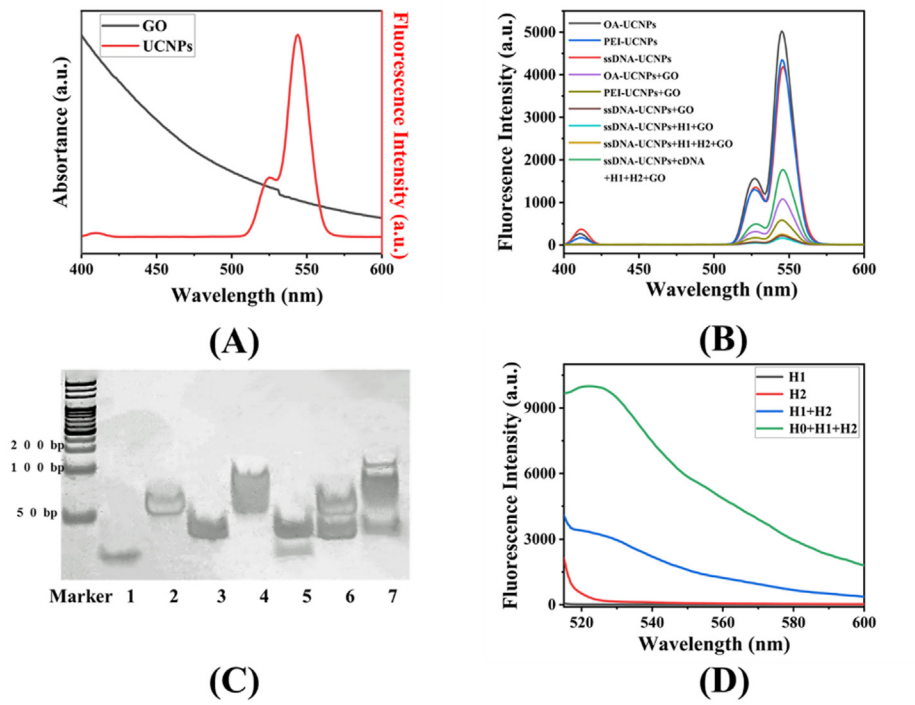

Fig. 4. (A) The fluorescence spectrum of UCNPs (red curve) and the ultraviolet absorbance range of graphene oxide (black curve); (B) Upconversion fluorescence spectra of OA-UCNPs, PEI-UCNPs, ssDNA-UCNPs, OA-UCNPs + GO, PEI-UCNPs + GO, ssDNA-UCNPs + GO, ssDNA-UCNPs + H1+GO, ssDNA-UCNPs + H1+H2+GO, and ssDNA-UCNPs + cDNA + H1+H2+GO, respectively. (C) Polyacrylamide gel electrophoresis diagram. Lane 1: H0, lane 2: H1, lane 3: H2, lane 4: H0+H1, lane 5: H0+H2, lane 6: H1+H2, lane 7: H0+H1+H2; (D) Fluorescence of FAM-labeled hairpin verified the feasibility of CHA. (For interpretation of the references to colour in this figure legend, the reader is referred to the Web version of this article.)

first step of the CHA amplification was successful. When H2 was mixed with H0 or H1, no new bands were observed (lanes 5 and 6), indicating that H2 was unsuccessful in coupling with H0 or H1. In addition, H1 and H2 maintained a stable hairpin structure without amplification (Refer to the software simulation diagram in Fig. S5). As shown in lane 7, in the presence of H0, the bands representing H1 and H2 gradually disappeared. Conversely, another higher band was observed, demonstrating that the successful composition of the H1—H2 duplex was carried out. Further verification of the feasibility of the CHA amplification was performed with fluorescence-recovery experiments. The fluorescein of 6-FAM and a quencher of BHQ-1 were modified at the sequence of F—H2, as shown in Fig. 4 (D). When H0 was present, H1 and F—H2 formed dsDNA, which created a distance between 6-FAM and BHQ-1, resulting in increased fluorescence intensity. In contrast to these findings, in the absence of H0, F—H2 maintained a hairpin structure, allowing 6-FAM to approach BHQ-1 and resulting in weakening of the overall fluorescence intensity.

3.4. Optimization of experimental conditions

The performance of the biosensor was affected by various parameters, such as the reaction conditions of MMPs and aptamers and the reaction conditions of UCNPs and GO. To increase the detection efficiency, various parameters were rationally optimized. Primarily, the aptamer contents on the MMPs were a critical factor in the assay system. Following the modification of the aptamers on MMPs, their content in the supernatant was subsequently decreased. As shown in Fig. 5 (A), when the amount of aptamer added exceeded 210 pmol, a significant increase was noted in its concentration in the supernatant, which resulted to the overloading of the aptamer modified on MMPs. Consequently, the amount of the aptamer added was selected as 210 pmol. The time required for the modification of the aptamer on the MMPs was of paramount importance. Fig. 5 (B) indicated that when the reaction time exceeded 2 h, the aptamer concentration in the supernatant was not significantly decreased. Therefore, the reaction time of the aptamers and MMPs was set at 2 h. The time of binding between the UCNPs and the CHA amplification products was also investigated. No apparent variation of the fluorescence intensity was observed following binding for 1 h (Fig. 5C), demonstrating that the integration of UCNPs and CHA amplification products was saturated. It was concluded that the reaction time of 1 h was the optimized time period. The GO content dominated the quenching efficiency of the UCNPs. When the amount of GO was 100 μL, the most ideal response was obtained as determined by the fluorescence spectrum (Fig. 5D). Therefore, 100 μL was used as the optimal amount of GO.

3.5. Fluorescence signal response of the detection method

Based on the optimization of the aforementioned experimental conditions, the present study assessed the linear relationship between the fluorescence of UCNPs and the concentration of FB1. In order to establish a standard curve, the fluorescence signal response of the biosensor was tested by detecting FB1 at different concentrations (0.032, 0.16, 0.8, 4, 20, 100, and 500 ng mL^{-1}). As shown in Fig. 6 (A), the logarithm of FB1 concentration range of 0.032—500 ng mL^{-1} exhibited an optimal linear relationship with the fluorescence intensity of UCNPs. Fig. 6 (B) indicated that the results of the linear equation fitting were $F = 163.8849lgC + 405.5395$ ($R^2 = 0.9971$) with a limit

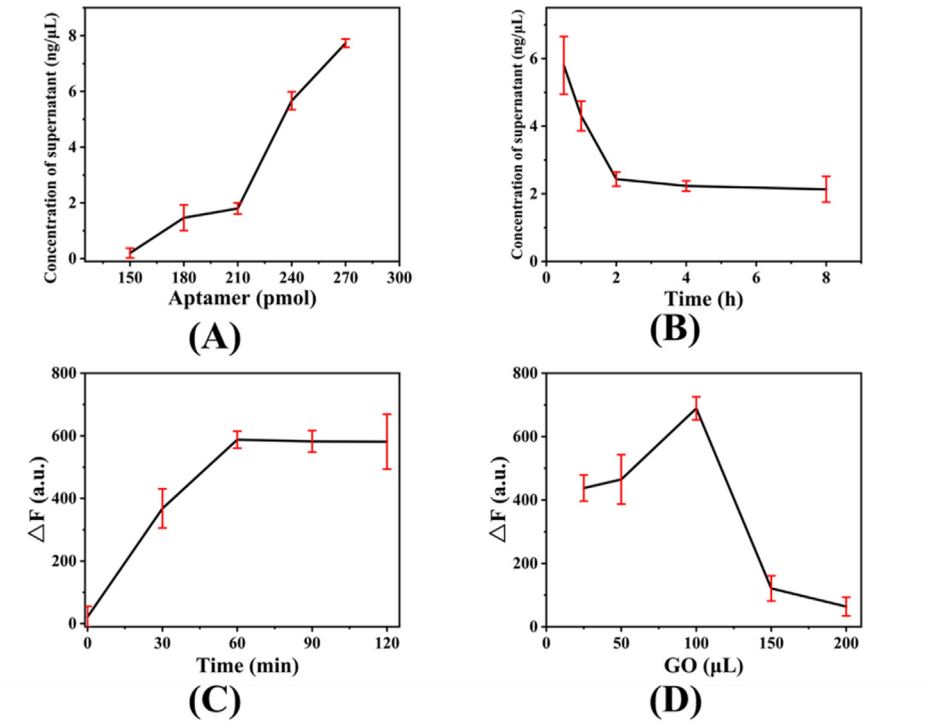

Fig. 5. Optimization of experimental conditions. (A) Amount of aptamer added; (B) Reaction time between the aptamer and MMPs; (C) Combination time of UCNPs and the amplified products of CHA; (D) Amount of GO added.

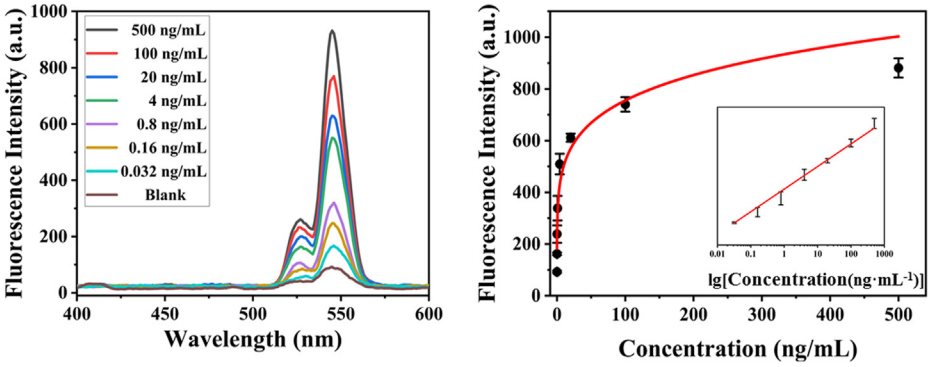

Fig. 6. Establishment of a standard curve. (A) Fluorescence response of UCNPs at different FB1 concentrations; (B) linear fitting equation of UCNPs-GO at different FB1 concentrations. In the inset, the abscissa is the logarithmic value of FB1 concentration, and the ordinate is the fluorescence intensity (a.u.).

of the detection of 0.0121 ng mL^{-1} (S/N = 3). Wu et al. directly constructed the UCNPs-Apt-GO system to detect FB1 without a signal amplification strategy. The sensitivity of the current method was an order of magnitude higher and exhibited a wider detection range compared with the method by Wu et al. [55].

3.6. Actual sample detection

To assess the practicability of the constructed sensor, three imported foods, including corn flour, oatmeal, and infant supplementary were used as samples for standard testing. The recovery

Table 1
Determination of FB1 in food samples by the method of the current study.

Samples	Spiking concentration (ng·mL^{-1})	Detected concentration (ng·mL^{-1})	Recovery ratio (%)	RSD (%)
corn flour	0.1	0.0952	95.2	3.2
	1	0.9971	99.7	3.1
	10	10.5340	105.3	2.4
Oatmeal	0.1	0.1024	102.4	3.8
	1	1.0320	103.2	2.8
	10	9.9786	99.8	3.2
infant supplement	0.1	0.0912	91.2	4.6
	1	0.9543	95.4	2.7
	10	10.3210	103.2	2.5

rate following the addition of the standards was shown in Table 1. The results indicated that the spiked recovery rates of corn flour, oat flour, and infant corn supplementary food were 95.2–105.3%, 99.8–103.2%, and 91.2–103.2%, respectively, suggesting that the sensor was suitable for accurate and sensitive detection of FB1 in unknown samples. The comparison with other methods was based on different detection principles (Table S2), demonstrating that the designed UCNPs-GO system based on the CHA signal amplification strategy was superior to the current commonly used methods for detecting FB1. The results of the ELISA kit for detecting FB1 in actual samples (Table S3) were similar to the proposed method, indicating that the accuracy of this method was acceptable.

3.7. Specificity of the detection method

In order to further evaluate the specificity of the biosensor, specific typical mycotoxins were selected as interfering substances for subsequent experiments. As shown in Fig. S6, at a concentration of 100 ng mL^{-1} for FB1 and interfering substances, the fluorescence response of this biosensor to interfering substances was significantly lower than that of FB1. The results demonstrated that the designed detection method exhibited optimal specificity.

4. Conclusion

In summary, the present study established an efficient and sensitive upconversion fluorescent sensing technology to detect trace amounts of FB1 in foods and verified that the nucleic acid signal amplification strategy could be efficiently applied to the field of food safety detection. UCNPs are provided with a long fluorescence lifetime, optimal chemical stability, and absence of background signal interference. Therefore, this allows them to be excellent carriers for signal output. In the present study, the CHA strategy was applied to the UCNPs-GO sensing system for the first time, by employing the interaction of GO and DNA with different structures. The FRET method was employed, leading to an improved detection ability of the UCNPs-GO system. The synthesis of more advanced UCNP materials, the replacement of various aptamers, and the design of diverse CHA structures can result to high-throughput, multi-purpose, and full-scene detection. In addition to assessing the levels of FB1 in food, the method of the present study can be used to detect FB1 during environmental monitoring and in clinical diagnosis.

Data and materials availability

All data required for the evaluation of the conclusions drawn in the current study are presented in the paper and/or the appendix.

CRediT authorship contribution statement

Yingkai Qin: conceived of the project. The manuscript was written through contributions of all authors. All authors have given approval to the final version of the manuscript. **Shuang Li:** Conceptualization, contributed to the conception, fabrication and writing of the manuscript. The manuscript was written through contributions of all authors. All authors have given approval to the final version of the manuscript. **Yu Wang:** contributed to the detection experiments. The manuscript was written through contributions of all authors. All authors have given approval to the final version of the manuscript. **Yuan Peng:** contributed to the principle design. The manuscript was written through contributions of all authors. All authors have given approval to the final version of the manuscript. **Dianpeng Han:** contributed to the principle design. The manuscript was written through contributions of all authors. All authors have given approval to the final version of the manuscript. **Huanying Zhou:** contributed to the manuscript modification. The manuscript was written through contributions of all authors. All authors have given approval to the final version of the manuscript. **Jialei Bai:** Data curation, contributed to data analysis. The manuscript was written through contributions of all authors. All authors have given approval to the final version of the manuscript. **Shuyue Ren:** contributed to figure processing. The manuscript was written through contributions of all authors. All authors have given approval to the final version of the manuscript. **Sen Li:** contributed to figure processing. The manuscript was written through contributions of all authors. All authors have given approval to the final version of the manuscript. **Ruipeng Chen:** contributed to the manuscript modification. The manuscript was written through contributions of all authors. All authors have given approval to the final version of the manuscript. **Tie Han:** Supervision, The manuscript was written through contributions of all authors. All authors have given approval to the final version of the manuscript. **Zhixian Gao:** Supervision, The manuscript was written through contributions of all authors. All authors have given approval to the final version of the manuscript.

Declaration of competing interest

The authors declare that they have no known competing financial interests or personal relationships that could influence the work reported in the current study.

Acknowledgment

This work was supported by the National Key Research and Development Program of China [No. 2018YFC1603500] for funding this research project.

Appendix A. Supplementary data

Supplementary data to this article can be found online at https://doi.org/10.1016/j.aca.2022.339811.

References

[1] T. Alsulami, N. Nath, R. Flemming, H. Wang, W. Zhou, J.H. Yu, Development of a novel homogeneous immunoassay using the engineered luminescent enzyme NanoLuc for the quantification of the mycotoxin fumonisin B1, Biosens. Bioelectron. 177 (2021) 112939.
[2] M. Eskola, G. Kos, C.T. Elliott, J. Hajšlová, S. Mayar, R. Krska, Worldwide contamination of food-crops with mycotoxins: validity of the widely cited 'FAO estimate' of 25, Crit. Rev. Food Sci. Nutr. 60 (16) (2020) 2773–2789.
[3] F. Wu, J.D. Groopman, J.J. Pestka, Public health impacts of foodborne mycotoxins, Annu. Rev. Food Sci. Technol. 5 (2014) 351–372.
[4] J. Kos, E. Janić Hajnal, A. Malachová, D. Steiner, M. Stranska, R. Krska, B. Poschmaier, M. Sulyok, Mycotoxins in maize harvested in Republic of Serbia in the period 2012-2015. Part 1: regulated mycotoxins and its derivatives, Food Chem. 312 (2020) 126034.
[5] C.P. Wild, J.D. Miller, J.D. Groopman, Mycotoxin Control in Low- and Middle-Income Countries, ed, vol. 9, International Agency for Research on Cancer, France, 2015.
[6] V. Ostry, F. Malir, J. Toman, Y. Grosse, Mycotoxins as human carcinogens-the IARC Monographs classification, Mycotoxin Res. 33 (1) (2017) 65–73.
[7] T. Yoshizawa, A. Yamashita, Y. Luo, Fumonisin occurrence in corn from high- and low-risk areas for human esophageal cancer in China, Appl. Environ. Microbiol. 60 (5) (1994) 1626–1629.
[8] H. Magoha, B. De Meulenaer, M. Kimanya, D. Hipolite, C. Lachat, P. Kolsteren, Fumonisin B1 contamination in breast milk and its exposure in infants under 6 months of age in Rombo, Northern Tanzania, Food Chem. Toxicol. 74 (2014) 112–116.
[9] M. Kamle, D.K. Mahato, S. Devi, K.E. Lee, S.G. Kang, P. Kumar, Fumonisins: impact on agriculture, food, and human health and their management strategies, Toxins 11 (6) (2019).
[10] Y.S. Li, Y. Zhou, S.Y. Lu, D.J. Guo, H.L. Ren, X.M. Meng, B.H. Zhi, C. Lin, Z. Wang, X.B. Li, Z.S. Liu, Development of a one-step test strip for rapid screening of fumonisins B1, B2 and B3 in maize, Food Control 24 (1–2) (2012) 72–77.

[11] X. Lin, X. Guo, Advances in biosensors, chemosensors and assays for the determination of Fusarium mycotoxins, Toxins 8 (6) (2016).
[12] M. Majdinasab, S. Ben Aissa, J.L. Marty, Advances in colorimetric strategies for mycotoxins detection: toward rapid industrial monitoring, Toxins 13 (1) (2020).
[13] I. Arranz, W.R. Baeyens, G. Van der Weken, S. De Saeger, C. Van Peteghem, Review: HPLC determination of fumonisin mycotoxins, Crit. Rev. Food Sci. Nutr. 44 (3) (2004) 195–203.
[14] S. Jaksic, M. Zivkov-Balos, Z. Mihaljev, Z. Masic, I. Jajic, N. Banic, B. Abramovic, Extraction without organic solvents in the determination of fumonisins B-1, B-2, and B-3 in maize by HPLC-FLD and ELISA tests, Food Anal. Methods 8 (6) (2015) 1446–1455.
[15] S. Tonti, M. Mandrioli, P. Nipoti, A. Pisi, T.G. Toschi, A. Prodi, Detection of fumonisins in fresh and dehydrated commercial garlic, J. Agric. Food Chem. 65 (32) (2017) 7000–7005.
[16] C. Wang, J. Qian, K. An, X. Huang, L. Zhao, Q. Liu, N. Hao, K. Wang, Magneto-controlled aptasensor for simultaneous electrochemical detection of dual mycotoxins in maize using metal sulfide quantum dots coated silica as labels, Biosens. Bioelectron. 89 (Pt 2) (2017) 802–809.
[17] Q. Zhou, Y. Lin, M. Xu, Z. Gao, H. Yang, D. Tang, Facile synthesis of enhanced fluorescent gold-silver bimetallic nanocluster and its application for highly sensitive detection of inorganic pyrophosphatase activity, Anal. Chem. 88 (17) (2016) 8886–8892.
[18] Z. Qiu, J. Shu, D. Tang, Bioresponsive release system for visual fluorescence detection of carcinoembryonic antigen from mesoporous silica nano-containers mediated optical color on quantum dot-enzyme-impregnated paper, Anal. Chem. 89 (9) (2017) 5152–5160.
[19] S. Lv, Y. Tang, K. Zhang, D. Tang, Wet NH(3)-triggered NH(2)-MIL-125(Ti) structural switch for visible fluorescence immunoassay impregnated on paper, Anal. Chem. 90 (24) (2018) 14121–14125.
[20] C. Wang, X. Huang, X. Tian, X. Zhang, S. Yu, X. Chang, Y. Ren, J. Qian, A multiplexed FRET aptasensor for the simultaneous detection of mycotoxins with magnetically controlled graphene oxide/Fe(3)O(4) as a single energy acceptor, Analyst 144 (20) (2019) 6004–6010.
[21] Y. Wang, Z. Li, T.J. Weber, D. Hu, C.T. Lin, J. Li, Y. Lin, In situ live cell sensing of multiple nucleotides exploiting DNA/RNA aptamers and graphene oxide nanosheets, Anal. Chem. 85 (14) (2013) 6775–6782.
[22] Y. Wang, Z. Li, D. Hu, C.T. Lin, J. Li, Y. Lin, Aptamer/graphene oxide nanocomplex for in situ molecular probing in living cells, J. Am. Chem. Soc. 132 (27) (2010) 9274–9276.
[23] X. Zhang, Y. Hu, X. Yang, Y. Tang, S. Han, A. Kang, H. Deng, Y. Chi, D. Zhu, Y. Lu, FÖrster resonance energy transfer (FRET)-based biosensors for biological applications, Biosens. Bioelectron. 138 (2019) 111314.
[24] L. Bao, K. Liu, Y. Chen, G. Yang, Construction of a rational-designed multifunctional platform based on a fluorescence resonance energy transfer process for simultaneous detection of pH and endogenous peroxynitrite, Anal. Chem. 93 (26) (2021) 9064–9073.
[25] I.O. Aparin, O.V. Sergeeva, A.S. Mishin, E.V. Khaydukov, V.A. Korshun, T.S. Zatsepin, Excimer-FRET cascade in dual DNA probes: open access to large Stokes shift, enhanced acceptor light up, and robust RNA sensing, Anal. Chem. 92 (10) (2020) 7028–7036.
[26] C. Guo, J. Zhai, Y. Wang, W. Yang, X. Xie, Wash-free detection of nucleic acids with photoswitch-mediated fluorescence resonance energy transfer against optical background interference, Anal. Chem. 93 (23) (2021) 8128–8133.
[27] Y. Li, L. Zhang, Z. Zhang, Y. Liu, J. Chen, J. Liu, P. Du, H. Guo, X. Lu, MnO(2) nanospheres assisted by cysteine combined with MnO(2) nanosheets as a fluorescence resonance energy transfer system for "Switch-on" detection of glutathione, Anal. Chem. 93 (27) (2021) 9621–9627.
[28] D. Tu, L. Liu, Q. Ju, Y. Liu, H. Zhu, R. Li, X. Chen, Time-resolved FRET biosensor based on amine-functionalized lanthanide-doped NaYF4 nanocrystals, Angew. Chem. Int. Ed. Engl. 50 (28) (2011) 6306–6310.
[29] X. Zhou, X. Xia, B.E. Smith, M.B. Lim, A.B. Bard, A. Pant, P.J. Pauzauskie, Interface-dependent radiative lifetimes of Yb(3+), Er(3+) Co-doped single NaYF(4) upconversion nanowires, ACS Appl. Mater. Interfaces 11 (25) (2019) 22817–22823.
[30] H. Chen, Y. Ding, Q. Yang, B. Barnych, G. González-Sapienza, B.D. Hammock, M. Wang, X. Hua, Fluorescent "turn off-on" small-molecule-monitoring nanoplatform based on dendrimer-like peptides as competitors, ACS Appl. Mater. Interfaces 11 (36) (2019) 33380–33389.
[31] B. Gu, M. Ye, L. Nie, Y. Fang, Z. Wang, X. Zhang, H. Zhang, Y. Zhou, Q. Zhang, Organic-dye-modified upconversion nanoparticle as a multichannel probe to detect Cu(2+) in living cells, ACS Appl. Mater. Interfaces 10 (1) (2018) 1028–1032.
[32] C. Hazra, V.N. Adusumalli, V. Mahalingam, 3,5-Dinitrobenzoic acid-capped upconverting nanocrystals for the selective detection of melamine, ACS Appl. Mater. Interfaces 6 (10) (2014) 7833–7839.
[33] H. Wang, Y. Li, M. Yang, P. Wang, Y. Gu, FRET-based upconversion nanoprobe sensitized by Nd(3+) for the ratiometric detection of hydrogen peroxide in vivo, ACS Appl. Mater. Interfaces 11 (7) (2019) 7441–7449.
[34] J.G. Jesu Raj, M. Quintanilla, K.A. Mahmoud, A. Ng, F. Vetrone, M. Zourob, Sensitive detection of ssDNA using an LRET-based upconverting nanohybrid material, ACS Appl. Mater. Interfaces 7 (33) (2015) 18257–18265.
[35] R. Li, Y. Li, M. Mu, B. Yang, X. Chen, W.Y.W. Lee, Y. Ke, W.H. Yung, B.Z. Tang, L. Bian, Multifunctional nanoprobe for the delivery of therapeutic siRNA and real-time molecular imaging of Parkinson's disease biomarkers, ACS Appl. Mater. Interfaces 13 (10) (2021) 11609–11620.
[36] X. Wang, J. Zhuang, Q. Peng, Y. Li, A general strategy for nanocrystal synthesis, Nature 437 (7055) (2005) 121–124.
[37] Z. Luo, L. Zhang, R. Zeng, L. Su, D. Tang, Near-infrared light-excited core-core-shell UCNP@Au@CdS upconversion nanospheres for ultrasensitive photoelectrochemical enzyme immunoassay, Anal. Chem. 90 (15) (2018) 9568–9575.
[38] Z. Qiu, J. Shu, D. Tang, NaYF(4):Yb,Er upconversion nanotransducer with in situ fabrication of Ag(2)S for near-infrared light responsive photoelectrochemical biosensor, Anal. Chem. 90 (20) (2018) 12214–12220.
[39] Z. Luo, Q. Qi, L. Zhang, R. Zeng, L. Su, D. Tang, Branched polyethylenimine-modified upconversion nanohybrid-mediated photoelectrochemical immunoassay with synergistic effect of dual-purpose copper ions, Anal. Chem. 91 (6) (2019) 4149–4156.
[40] W. Bian, Y. Lin, T. Wang, X. Yu, J. Qiu, M. Zhou, H. Luo, S.F. Yu, X. Xu, Direct identification of surface defects and their influence on the optical characteristics of upconversion nanoparticles, ACS Nano 12 (4) (2018) 3623–3628.
[41] C. Zeng, N. Lu, Y. Wen, G. Liu, R. Zhang, J. Zhang, F. Wang, X. Liu, Q. Li, Z. Tang, M. Zhang, Engineering nanozymes using DNA for catalytic regulation, ACS Appl. Mater. Interfaces 11 (2) (2019) 1790–1799.
[42] J. Tian, H. Chu, Y. Zhang, K. Li, H. Tian, X. Zhang, W. Xu, TiO(2) nanoparticle-enhanced linker recombinant strand displacement amplification (LRSDA) for universal label-free visual bioassays, ACS Appl. Mater. Interfaces 11 (50) (2019) 46504–46514.
[43] P. Chen, X. Jiang, K. Huang, P. Hu, X. Li, L. Wei, W. Liu, L. Wei, C. Tao, B. Ying, X. Wei, J. Geng, Multimode MicroRNA sensing via multiple enzyme-free signal amplification and cation-exchange reaction, ACS Appl. Mater. Interfaces 11 (40) (2019) 36476–36484.
[44] H. Li, J. Wang, X. Wang, H. Lin, F. Li, Perylene-based photoactive material as a double-stranded DNA intercalating probe for ultrasensitive photoelectrochemical biosensing, ACS Appl. Mater. Interfaces 11 (18) (2019) 16958–16964.
[45] R. Asadi, H. Mollasalehi, The mechanism and improvements to the isothermal amplification of nucleic acids, at a glance, Anal. Biochem. 631 (2021) 114260.
[46] B. Özay, S.E. McCalla, A review of reaction enhancement strategies for isothermal nucleic acid amplification reactions, Sens. Actuators Rep. 3 (2021) 100033.
[47] N. Yin, S. Yuan, M. Zhang, J. Wang, Y. Li, Y. Peng, J. Bai, B. Ning, J. Liang, Z. Gao, An aptamer-based fluorometric zearalenone assay using a lighting-up silver nanocluster probe and catalyzed by a hairpin assembly, Mikrochim. Acta 186 (12) (2019) 765.
[48] W. Zhou, X. Gong, Y. Xiang, R. Yuan, Y. Chai, Target-triggered quadratic amplification for label-free and sensitive visual detection of cytokines based on hairpin aptamer DNAzyme probes, Anal. Chem. 86 (1) (2014) 953–958.
[49] P. Yin, H.M. Choi, C.R. Calvert, N.A. Pierce, Programming biomolecular self-assembly pathways, Nature 451 (7176) (2008) 318–322.
[50] Y. Wu, C. Fu, W. Shi, J. Chen, Recent advances in catalytic hairpin assembly signal amplification-based sensing strategies for microRNA detection, Talanta 235 (2021) 122735.
[51] X. Liu, X. Zhou, X. Xia, H. Xiang, Catalytic hairpin assembly-based double-end DNAzyme cascade-feedback amplification for sensitive fluorescence detection of HIV-1 DNA, Anal. Chim. Acta 1096 (2020) 159–165.
[52] J. Liu, Z. Sun, Y. Deng, Y. Zou, C. Li, X. Guo, L. Xiong, Y. Gao, F. Li, D. Zhao, Highly water-dispersible biocompatible magnetite particles with low cytotoxicity stabilized by citrate groups, Angew. Chem. Int. Ed. Engl. 48 (32) (2009) 5875–5879.
[53] Y. Rong, H. Li, Q. Ouyang, S. Ali, Q. Chen, Rapid and sensitive detection of diazinon in food based on the FRET between rare-earth doped upconversion nanoparticles and graphene oxide, Spectrochim. Acta Mol. Biomol. Spectrosc. 239 (2020) 118500.
[54] X. Chen, J. Lan, Y. Liu, L. Li, L. Yan, Y. Xia, F. Wu, C. Li, S. Li, J. Chen, A paper-supported aptasensor based on upconversion luminescence resonance energy transfer for the accessible determination of exosomes, Biosens. Bioelectron. 102 (2018) 582–588.
[55] S. Wu, N. Duan, X. Ma, Y. Xia, H. Wang, Z. Wang, Q. Zhang, Multiplexed fluorescence resonance energy transfer aptasensor between upconversion nanoparticles and graphene oxide for the simultaneous determination of mycotoxins, Anal. Chem. 84 (14) (2012) 6263–6270.